

Optimizing Auto-correlation for Fast Target Search in Large Search Space

Arif Mahmood, Ajmal Mian and Robyn Owens

This work has been submitted to the IEEE for possible publication. Copyright may be transferred without notice, after which this version may no longer be accessible

Abstract—In remote sensing image-blurring is induced by many sources such as atmospheric scatter, optical aberration, spatial and temporal sensor integration. The natural blurring can be exploited to speed up target search by fast template matching. In this paper, we synthetically induce additional non-uniform blurring to further increase the speed of the matching process. To avoid loss of accuracy, the amount of synthetic blurring is varied spatially over the image according to the underlying content. We extend transitive algorithm for fast template matching by incorporating controlled image blur. To this end we propose an Efficient Group Size (EGS) algorithm which minimizes the number of similarity computations for a particular search image. A larger efficient group size guarantees less computations and more speedup. EGS algorithm is used as a component in our proposed Optimizing auto-correlation (OptA) algorithm. In OptA a search image is iteratively non-uniformly blurred while ensuring no accuracy degradation at any image location. In each iteration efficient group size and overall computations are estimated by using the proposed EGS algorithm. The OptA algorithm stops when the number of computations cannot be further decreased without accuracy degradation. The proposed algorithm is compared with six existing state of the art exhaustive accuracy techniques using correlation coefficient as the similarity measure. Experiments on satellite and aerial image datasets demonstrate the effectiveness of the proposed algorithm.

Index Terms—Fast Template Matching, Fast Pattern Matching, Large Search Space, Transitivity of Correlation, Auto-correlation

I. INTRODUCTION

Fast template or pattern matching [1], [2], [3] is a critical step in many remote sensing applications such as object detection and recognition [4], [5], [6], [7], [8], image registration and alignment [9], [2], [10], glacier surface movement detection [11], [12], road detection [13], seismic monitoring [14], shadow detection [15], cloud detection and tracking [16], sea ice tracking [17], [18], stereo image matching for space born imagery [19], DEM generation [20], image super resolution [5], and content based image retrieval [21], [22]. In template matching, a smaller template or target image is matched at multiple locations of a larger search image to find the best match location that maximizes an appropriate similarity measure.

In most of the remote sensing applications, the search space is large which increases the computational complexity of the matching process. Numerous techniques have been proposed

in literature to make the matching process fast. Based on the search accuracy, these approaches may be broadly divided into approximate accuracy and exhaustive accuracy techniques. The first category obtains fast speedup at the cost of some loss of accuracy and often incorporates one or more approximations. For example, the search space may be approximated with a smaller search space, the target may be approximated with a simple representation, or the similarity measure approximated with a simpler measure. The exhaustive accuracy techniques obtain fast speedup without losing accuracy. This category includes domain transformation techniques using FFT and bound based computation elimination algorithms in which unsuitable search locations are skipped from computations. In this paper we argue on maintaining exhaustive accuracy in the proposed algorithm which skips unsuitable search locations based on bound comparisons. To make the process fast, the search image is processed in a controlled way to avoid any loss of accuracy.

Bound based computation elimination algorithms are exhaustive accuracy fast template matching techniques. Most of these algorithms are based on the Sum of Absolute Differences (SAD) or the Sum of Squared Differences (SSD) [23], [24], [25]. Elimination algorithms using similarity measures invariant to the intensity and contrast variations such as Normalized Cross Correlation (NCC) or Correlation Coefficient (ρ) (or Zero-mean NCC) are relatively few including [26], [27], [28]. Algorithms in this category are the main focus of this paper. In most of the remote sensing applications, the images to be matched are acquired at different time of the day, often with significant time lag. Therefore simple measures like SAD and SSD are more vulnerable to errors as compared to the Correlation Coefficient.

Correlation coefficient (ρ) (or ZNCC) is more robust to the linear photo-metric variations between the two images to be matched. Correlation coefficient between template image t and a location in search image r_o is denoted as ρ_{to} and defined as

$$\rho_{to} = \sum_{x,y} \frac{(t(x,y) - \mu_t)(r_o(x,y) - \mu_o)}{\sigma_t \sigma_o}, \quad (1)$$

$$\sigma_t = \sqrt{\sum_{x,y} (t(x,y) - \mu_t)^2}, \sigma_o = \sqrt{\sum_{x,y} (r_o(x,y) - \mu_o)^2},$$

where μ_t and μ_o are the means of t and r_o respectively. If $\{r_c, r_o\} \in \mathcal{R}^{m \times n}$ are two shifted blocks in the same image,

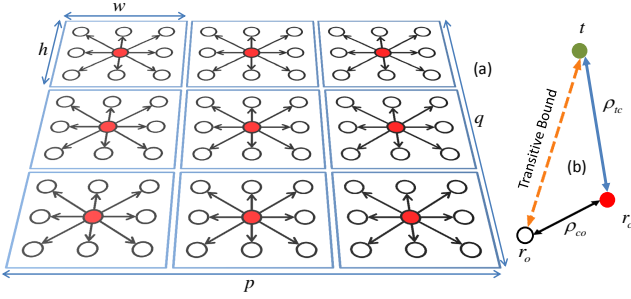


Fig. 1. (a) Contiguous search locations in the reference image $I \in \mathcal{R}^{p \times q}$ form groups of size $h \times w$. (b) Two known correlations $\rho_{tc} = \rho(t, r_c)$ and $\rho_{co} = \rho(r_c, r_o)$ bound the unknown correlation $\rho_{to} = \rho(t, r_o)$.

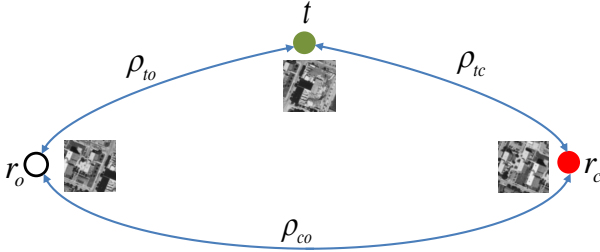


Fig. 2. Transitive bounds given by Theorem 1 are defined on three image blocks $\{t, r_o, r_c\} \in \mathcal{R}^{m \times n}$ and are quadratic in shape. If $\rho_{co} = 0.81$ and $\rho_{tc} = 0.61$ then third side is bounded by $0.017 \leq \rho_{to} \leq 0.955$.

then ρ_{co} in (1) will represent local auto-correlation with a shift s . In this paper we use local auto-correlation to speedup the matching process. Local auto-correlation is enhanced by inducing controlled non-uniform image blur in the search images. As a result, we obtain high matching speed with a robust match measure.

In the category of correlation coefficient based fast template matching algorithms, we consider transitive algorithm (TEA) [28] mainly because this algorithm gives the opportunity to incorporate non-uniform blur to obtain high speed template matching. Also TEA has been shown to be faster than the previous algorithms of the same category [28]. However, TEA cannot be directly used for this purpose because the design parameters of this algorithm are currently user defined. Especially the group size parameter and the initial threshold. We develop an Efficient Group Size (EGS) algorithm which maximizes an estimation of the the eliminated computations over group size parameter. We then incorporate EGS algorithm within a novel algorithm for optimization of auto-correlation (OptA) which computes non-uniformly blurred search image. A scheme for early detection of the high initial threshold is also proposed. All these algorithms combined with TEA make a fast template matching system which has the same accuracy as the original algorithm but obtains significant speedup. Experiments are performed with a wide variety of the template images on real satellite and aerial image datasets. We observe significant speedup over existing techniques.

II. A REVIEW OF TRANSITIVE ELIMINATION ALGORITHM

In transitive algorithm the search image is divided into small groups of contiguous search locations. Local auto-correlation

of the group center is computed with all other locations within that group and transitive bounds are computed. At run time, the template image is only matched with the group center, while transitive bounds are used to skip all other unlikely locations (Fig. 1).

Transitive bounds [28] are defined for three images, template t , outer block r_o and central block r_c . Pairwise correlations are given by $\{\rho_{to}, \rho_{tc}, \rho_{co}\}$ (Fig. 2). Each correlation is bounded by the other two correlations by the transitive inequality. Considering ρ_{to} as bounded correlation and the other two as bounding correlations, the upper bound is given by

$$\rho_{to} \leq \rho_{tc}\rho_{co} + \sqrt{(1 - \rho_{tc}^2)(1 - \rho_{co}^2)}, \quad (2)$$

and the lower bound is given by

$$\rho_{to} \geq \rho_{tc}\rho_{co} - \sqrt{(1 - \rho_{tc}^2)(1 - \rho_{co}^2)}. \quad (3)$$

Transitive Gap ϵ is the difference between the upper and the lower transitive bounds

$$\epsilon = 2\sqrt{1 - \rho_{tc}^2}\sqrt{1 - \rho_{co}^2} \quad (4)$$

We observe that ρ_{to} is contained within the transitive gap. The bound tightness can be defined as: the smaller the transitive gap (ϵ), the tighter the transitive bounds.

Proposition 2.1: Transitive gap ϵ will be minimized if the magnitude of at least one of the two bounding correlations $\{\rho_{tc}, \rho_{co}\}$ is maximized.

Proof Taking the derivative of ϵ w.r.t any one of the two bounding correlations and setting it equal to zero $\partial\epsilon/\partial\rho_{tc} = 0$. From 4 we get

$$\frac{\partial}{\partial\rho_{tc}}(\rho_{tc}^2\rho_{co}^2 - (\rho_{tc}^2 + \rho_{co}^2) + 1) = 0.$$

$\rho_{tc}(1 - \rho_{co}^2) = 0$. Since $\rho_{tc} \neq 0$ therefore $\rho_{co}^2 = 1$ or $\rho_{co} \rightarrow \pm 1$.

In the remote sensing images, consecutive search locations are often highly correlated, therefore the nearby search locations can be grouped such that intra-group auto-correlations remain high. Fig. 1 shows the search image I divided into groups of $h \times w$ search locations. Each group has a central location (r_c) and others are outer locations (r_o). Auto-correlation of each outer location r_o with the group center r_c is computed by using a very efficient Algorithm 1. At run time, the template image (t) is only matched with r_c , while the remaining locations r_o can be skipped if the sufficient elimination condition given below is satisfied.

Sufficient Elimination Condition: without loss of accuracy, a search location $r_o \in I$ can be skipped if there exists another search location $r_b \in I$ such that

$$\rho_{tb} \geq \rho_{tc}\rho_{co} + \sqrt{1 - \rho_{tc}^2}\sqrt{1 - \rho_{co}^2}, \quad (5)$$

where ρ_{tb} is the correlation coefficient (1) between t and $r_b \in \mathcal{R}^{m \times n}$.

If the sufficient elimination condition is satisfied then it is guaranteed that $\rho_{tb} \geq \rho_{to}$, therefore r_o cannot exhibit better similarity than r_b .

Algorithm 1 Local Auto-correlation Computation Algorithm

Input: $I \in \mathcal{R}^{p \times q}$, (m, n) Template size, (h, w) Group Size

Output: Auto-correlation Matrix $R_{co} \in \mathcal{R}^{p \times q}$

```

for  $i \leftarrow 1$  to  $h$  do
  for  $j \leftarrow 1$  to  $w$  do
    for  $\forall(x, y) \in I$  do
       $P(x, y) \leftarrow I(x, y) * I(x + i, y + j)$ 
    end for
     $S \leftarrow \text{Running-Sum}(P, m, n)$ 
    for  $\forall(x, y) \in \text{Group Centers}$  do
       $R_{co}(x + i, y + j) \leftarrow S(x + m, y + n)$ 
       $x \leftarrow x + h$ 
       $y \leftarrow y + w$ 
    end for
  end for
end for

```

III. COMPUTING COMPUTATIONAL COSTS

In this section we analyze different types of costs involved in the transitive algorithm. These costs include the auto-correlation cost, central correlation cost and the cost of computing correlation on the locations with failed elimination condition. Based on this analysis, we develop an efficient group size algorithm which takes as input the auto-correlation matrix, initial threshold and computes a group size that minimizes the sum of all costs.

A. Local Auto-correlation Computational Cost (c_a)

Auto-correlation is efficiently computed by algorithm 1. The reference image is multiplied with its shifted versions and running sum approach is used to compute the sum of products over each block requiring only four operations. The overall complexity of this algorithm is $O((hw-1)pq)$, where $h \times w$ is the group size or the number of shifts applied to the reference image. Note that this cost is significantly smaller than the cost of a single template matching $O(mnpq)$, because $hw \ll mn$.

B. Central Locations Correlation Cost (c_c)

Central correlation cost c_c is required to match the template image t with the group centers r_c , therefore c_c is proportional to the number of groups in the search image

$$c_c = c_p \frac{pq}{hw}, \quad (6)$$

where c_p is the one time matching cost. c_c remains fixed for a particular group size $h \times w$ and can be reduced by increasing the group size.

C. Retained Locations Correlation Cost (c_r)

This is the cost of computing the correlation at the locations with failed sufficient elimination condition: $c_r = c_p n_r$, where n_r are the number of retained locations. As the group size increases the within group auto-correlation reduces due to increased distance between r_c and r_o . As a result, the transitive bound becomes loose, causing the sufficient elimination condition to fail more often and an increase in c_r . A

relatively precise estimate of retained locations can be found by Proposition 3.1 while a relaxed but easy to pre-compute estimate can be found by Proposition 3.2.

Proposition 3.1: For a fixed threshold value ρ_{tb} , the sufficient elimination condition will be satisfied on all search locations with auto-correlation ρ_{co} satisfying the following inequality

$$\rho_{co} \geq \rho_{tb} \rho_{tc} + \sqrt{1 + \rho_{tc}^2 \rho_{tb}^2 - (\rho_{tc}^2 + \rho_{tb}^2)}.$$

Proof Elimination will be obtained if

$$\rho_{tb} - \rho_{co} \rho_{tc} \geq \sqrt{1 - \rho_{co}^2} \sqrt{1 - \rho_{tc}^2}, \quad (7)$$

or simplifying,

$$\rho_{co}^2 - 2\rho_{tb}\rho_{tc}\rho_{co} + (\rho_{tc}^2 + \rho_{tb}^2 - 1) \geq 0. \quad (8)$$

Being quadratic, ρ_{co} has two roots. In the practically useful ranges of ρ_{tc} and ρ_{tb} , the upper root mostly remains positive while the lower root is mostly negative. Since auto-correlation of the natural images for small lags is positive ($\rho_{co} \geq 0$) therefore in most of the cases only the upper root is the valid solution. Hence elimination will be obtained if ρ_{co} is larger than the upper root:

$$\rho_{co} \geq \rho_{tb} \rho_{tc} + \sqrt{1 + \rho_{tc}^2 \rho_{tb}^2 - (\rho_{tc}^2 + \rho_{tb}^2)}. \quad (9)$$

Note that in narrow ranges, lower root may also become positive resulting in more elimination than the estimation based on (9). However, these cases being less frequent may be ignored from the estimation without inducing significant error. Proposition 3.1 can be used to estimate the number of search locations with failed elimination condition if ρ_{tc} is known which limits the beforehand estimation of the retained locations. However, Proposition 3.2 enables us to estimate the number of retained locations without knowing ρ_{tc} . We empirically observe that the estimation error in Proposition 3.2 is small and the result is used to formulate the efficient group size algorithm.

Proposition 3.2: A search location will be eliminated if

$$E[\rho_{co}] \geq \sqrt{1 - \rho_{tb}^2},$$

where the expectation is computed over a neighborhood around that location.

Proof Taking expectation of both sides of (9) and considering ρ_{tb} as a fixed value,

$$E[\rho_{co}] \geq \rho_{tb} E[\rho_{tc}] + \sqrt{1 - \rho_{tb}^2} E[\sqrt{1 - \rho_{tc}^2}].$$

Since t is uncorrelated with most of the search locations in I , therefore $E[\rho_{tc}] = 0$.

$$E[\rho_{co}] \geq \sqrt{1 - \rho_{tb}^2} E[\sqrt{1 - \rho_{tc}^2}]. \quad (10)$$

Taylor series expansion of $\sqrt{1 - \rho_{tc}^2}$ centered at 1 is

$$\sqrt{1 - \rho_{tc}^2} \approx 1 + \frac{\rho_{tc}^2}{2} - \frac{\rho_{tc}^4}{8}. \quad (11)$$

Since $-1 \leq \rho_{tc} \leq 1$, therefore $\frac{\rho_{tc}^2}{2} - \frac{\rho_{tc}^4}{8} \geq 0$.

$$E[\sqrt{1 - \rho_{tc}^2}] \geq 1. \quad (12)$$

Algorithm 2 EGS: Efficient Group Size

Input: $I \in \mathcal{R}^{p \times q}$, (h_0, w_0) {Initial Group Size}, (m, n) {Template Size}, ρ_{th} {Threshold}, ξ {Cost decrement}

Output: (h_e, w_e) , R_{co} , c_t {Total estimated Cost}

$$c_t^0 \leftarrow mnpq, k \leftarrow 1, c_t^1 \leftarrow 0$$

while $c_t^{k-1} - c_t^k > \xi$ **do**

$$c_c^k = (pq)/(h_k w_k)$$

$$R_{co}^k \leftarrow \text{Auto-correlation}(I, m, n, h_k, w_k)$$

for $\forall(x, y) \in I$ **do**

if $R_{co}^k(x, y) < \sqrt{1 - \rho_{tb}^2}$ **then**

$$c_r^k \leftarrow c_r^k + 1$$

end if

end for

$$c_t^k \leftarrow c_\rho(c_r^k + c_c^k)$$

if $c_t^{k-1} - c_t^k > \xi$ **then**

$$c_t^{k-1} \leftarrow c_t^k, h_{k-1} \leftarrow h_k, w_{k-1} \leftarrow w_k$$

$$h_k \leftarrow h_k + \Delta h, w_k \leftarrow w_k + \Delta w$$

end if

$$k \leftarrow k + 1$$

end while

$$c_t \leftarrow c_t^{k-1}, R_{co} \leftarrow R_{co}^{k-1}, \{h_e, w_e\} \leftarrow \{h_{k-1}, w_{k-1}\}$$

Probability around $\rho_{tc} = 0$ is very high and probability around $|\rho_{tc}| = 1$ is very low. Therefore, most of the times $\rho_{tc}^4/8$ will have a negligibly small magnitude.

$$E[\sqrt{1 - \rho_{tc}^2}] \leq 1 + \frac{1}{2}E[\rho_{tc}^2].$$

Note that ρ_{tc}^2 is the coefficient of determination [29]. If the two sets of numbers have normal distribution, and are uncorrelated the coefficient of determination will have a Beta distribution [30], [31]. The mean of this distribution for the univariate case is $1/(mn - 1)$. Therefore

$$E[\sqrt{1 - \rho_{tc}^2}] \leq 1 + \frac{1}{2(mn - 1)}.$$

For large mn , $\frac{1}{2(mn - 1)} \approx 0$, therefore

$$E[\sqrt{1 - \rho_{tc}^2}] \leq 1 \quad (13)$$

From (12) and (13), we conclude

$$E[\sqrt{1 - \rho_{tc}^2}] = 1. \quad (14)$$

Therefore (10) gets simplified to

$$E[\rho_{co}] \leq \sqrt{1 - \rho_{tb}^2}$$

Using Proposition 3.2, an estimate of the correlation cost (c_r) on the search locations (n_r) where sufficient elimination condition may fail is given by

$$c_r = c_\rho n_r = c_\rho \sum_{x=1}^p \sum_{y=1}^q (\rho_{co}(x, y) \leq \sqrt{1 - \rho_{tb}^2}), \quad (15)$$

where $(\rho_{co}(x, y) \leq \sqrt{1 - \rho_{tb}^2})$ will evaluate 1 if true and 0 if false.

Total cost c_t is given by the sum of the auto-correlation, central locations and the retained locations cost: $c_t = c_c +$

$c_r + \frac{c_a}{n_t}$, where n_t is the number of template images to be matched with the same reference image. For large n_t , the auto-correlation cost factor $\frac{c_a}{n_t}$ will become very small and can be ignored. Therefore, total cost is given by

$$c_t = c_\rho \left(\frac{pq}{hw} + n_r \right). \quad (16)$$

D. Computing Efficient Group Size

We define efficient group size (w_e, h_e) as

$$\{w_e, h_e\} := \min_{h, w} c_\rho \left(\frac{pq}{hw} + n_r \right) \quad (17)$$

As the group size increases the total cost given by (17) decreases until it hits the minimum and then starts increasing. As the gradient of the cost function changes sign, efficient group size parameters are found. Algorithm 2 iteratively solves this optimization problem. In k^{th} iteration within group auto-correlation matrix R_{co}^k is computed using Algorithm 1. In each iteration, the computational complexity of Algorithm 1 is $O((h_k w_k - 1)pq)$, where (h_k, w_k) is the group size in that iteration. Total computational complexity is of the order of $O(\omega pq)$, where $\omega = f((h_o + h_f)(w_o + w_f)/4 - 1)$, f is the number of iterations, (h_o, w_o) are the initial and (h_f, w_f) are final group sizes. In order to ensure that the next iteration only gets executed if the decrease in cost was significant from the last iteration, a parameter ξ is introduced. In our experiments, we fix the value of ξ to 0.5% of the total cost in the last iteration.

IV. PREVENTING LOSS OF SIGNAL DETECTION DUE TO BLUR

Search image may be blurred to improve auto-correlation (ρ_{co}) resulting in larger efficient group size and hence more speedup. However, uncontrolled blurring may suppress the peaks resulting in the loss of detection rendering the algorithm less accurate than the exhaustive accuracy. We propose to perform controlled non-uniform blurring in different image regions such that speedup is obtained without compromising exhaustive accuracy.

In order to produce image blur, each pixel in the image I is replaced by a weighted average of the pixels in a small neighborhood around it called *blur support*. Let \hat{I} be a blurred image computed as

$$\hat{I}(x, y) = \sum_{i=-d}^d \sum_{j=-d}^d w(i, j) I(x + i, y + j), \quad (18)$$

where $1 \geq w(i, j) \geq 0$ is a weight function or spatial averaging filter of size $(2d + 1) \times (2d + 1)$ which is the blur support. There are many types of blur filters however the Gaussian averaging mask is most commonly used.

$$w(i, j) = \frac{1}{\alpha_g} \exp\left(-\frac{i^2 + j^2}{2\sigma_g^2}\right), \quad (19)$$

where α_g is a normalization term which ensures $\sum w(i, j) = 1$ and σ_g is Gaussian variance which controls the weight distribution and the filter size. In (19), the amount of blur depends on the parameter σ_g which controls the weight distribution and

the filter size parameter d is given by $\sqrt{-2\sigma_g \ln(t_g)}$, where t_g is the minimum non zero filter value.

The correlation of t with blur image location $\hat{r}_o \in \hat{I}$, represented by $\hat{\rho}_{to}$, is a weighted average of correlations of t with original image blocks $r_o\{i, j\}$ over the blur support. As the blur support increases, correlation peaks with smaller base suffer more averaging as compared to the broader peaks. This may result in three types of accuracy de-gradations including incorrect detection due to suppression of the correct peak (signal) below a noise peak, lack of detection due to suppression of the signal below the initial threshold and the loss of localization due to widening of the signal peak. The first type of degradation may happen if a competitive noise peak with bigger support is present in the search space.

A. Suppression of the Signal to Noise Ratio

We argue that for the correct peaks (signal) with support larger than the blur support, the blur process cannot suppress the signal below the noise peaks.

Proposition 4.1: Suppose there exists two search locations $\{r_a, r_b\} \in I$ such that $\rho_{at} > \rho_{bt}$. After blur $\hat{\rho}_{at} > \hat{\rho}_{bt}$ is guaranteed if

$$\min_{-d \leq (i,j) \leq d} \{\rho_{at}\{i, j\}\} \geq \max_{-d \leq (u,v) \leq d} \{\rho_{bt}\{u, v\}\}. \quad (20)$$

Proof Consider two weight matrices $\{\nu_a, \nu_b\} \in \mathcal{R}^{(2d+1) \times (2d+1)}$ such that $1 > \{\nu_a(i, j), \nu_b(u, v)\} > 0$, $\sum_{i,j} \nu_a(i, j) = \sum_{u,v} \nu_b(u, v) = 1$ and in general $\nu_a(i, j) \neq \nu_b(u, v)$. By the linearity property

$$\sum_{i,j} \nu_a(i, j) \rho_{at}\{i, j\} \geq \sum_{u,v} \nu_b(u, v) \rho_{bt}\{u, v\}.$$

We now show that the weight matrices derived from the blurring filters satisfy the sum to 1 property. If the variances of the blurred images are $\hat{\sigma}_a$ and $\hat{\sigma}_b$, the weight matrices will be given by

$$\nu_a(i, j) = \frac{w(i, j)\sigma_a\{i, j\}}{\hat{\sigma}_a}, \nu_b(u, v) = \frac{w(u, v)\sigma_b\{u, v\}}{\hat{\sigma}_b}.$$

Since the remotely sensed images often have high local auto-correlation, the blurred image variances simplify to

$$\hat{\sigma}_a \approx \sum_{i,j} w(i, j)\sigma_a\{i, j\} \text{ and } \hat{\sigma}_b \approx \sum_{u,v} w(u, v)\sigma_b\{u, v\}.$$

Substitution of these values yields following weight matrices

$$\nu_a(i, j) = \frac{w(i, j)\sigma_a\{i, j\}}{\sum_{i',j'} w(i', j')\sigma_a\{i', j'\}}, \quad (21)$$

$$\nu_b(u, v) = \frac{w(u, v)\sigma_b\{u, v\}}{\sum_{u',v'} w(u', v')\sigma_b\{u', v'\}}, \quad (22)$$

where (i', j') are the dummy variables of summation. Therefore $\sum_{i,j} \nu_a(i, j) = \sum_{u,v} \nu_b(u, v) = 1$, which proves $\hat{\rho}_{at} > \hat{\rho}_{bt}$.

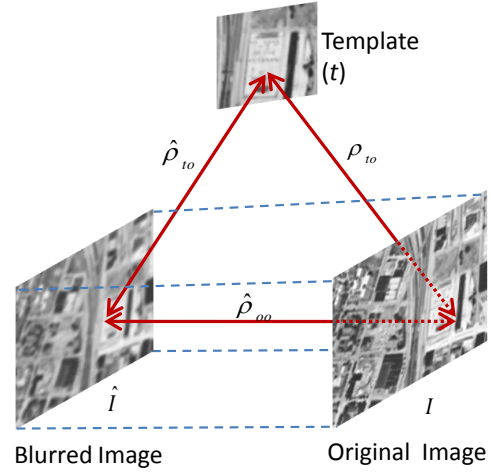


Fig. 3. Using transitive bounds for image quality preservation (Prop. 4.3)

B. Loss of Signal Detection

Let ρ_{mt} be the correlation maximum in the original image and $\hat{\rho}_{mt}$ be the corresponding maximum in the blur image. Loss of signal detection may occur if $\rho_{mt} > \rho_{th}$ but $\hat{\rho}_{mt} < \rho_{th}$ where ρ_{th} is the initial correlation threshold.

Corollary 4.2: If $\rho_{mt} > \rho_{th}$, after blur $\hat{\rho}_{mt} > \rho_{th}$ is guaranteed if

$$\min_{-d \leq (i,j) \leq d} \{\rho_{mt}\{i, j\}\} \geq \rho_{th}. \quad (23)$$

Proof Follows from Proposition 4.1.

One may expect a reduction in correlation between t and \hat{r}_o due to blurring $\hat{\rho}_{to} \leq \rho_{to}$, however the reduction can be constrained by using the lower transitive bound.

Proposition 4.3: If $\rho_{to} > \rho_{th}$ then $\hat{\rho}_{to} > \rho_{th}$ is guaranteed if

$$\hat{\rho}_{oo} \geq \rho_{th}\rho_{to} + \sqrt{1 + \rho_{th}^2\rho_{to}^2 - (\rho_{th}^2 + \rho_{to}^2)}, \quad (24)$$

where $\hat{\rho}_{oo}$ is the correlation coefficient between the original image block r_o and its blurred version \hat{r}_o .

Proof From Fig. 3

$$\hat{\rho}_{to} \geq \hat{\rho}_{oo}\rho_{to} - \sqrt{1 - \hat{\rho}_{oo}^2}\sqrt{1 - \rho_{to}^2}, \quad (25)$$

$\hat{\rho}_{to} > \rho_{th}$ will be guaranteed if

$$\hat{\rho}_{oo}\rho_{to} - \sqrt{1 - \hat{\rho}_{oo}^2}\sqrt{1 - \rho_{to}^2} \geq \rho_{th}. \quad (26)$$

Squaring both sides and simplifying:

$$\hat{\rho}_{oo}^2 - 2\rho_{th}\hat{\rho}_{oo}\rho_{to} + (\rho_{th}^2 + \rho_{to}^2 - 1) \geq 0, \quad (27)$$

which is quadratic in $\hat{\rho}_{oo}$ and only one root satisfies (26). For all values of $\hat{\rho}_{oo} \geq$ this root, Proposition 4.3 will be satisfied.

Note that only the suppression of the maximum peak (signal) below the threshold degrades accuracy. Therefore, putting $\rho_{to} = \rho_{\max}$ in (24)

$$\hat{\rho}_{oo} \geq \rho_{th}\rho_{\max} + \sqrt{1 + \rho_{th}^2\rho_{\max}^2 - (\rho_{th}^2 + \rho_{\max}^2)} \quad (28)$$

To avoid miss detection, (28) is ensured to hold for all search locations. We propose a very efficient method for the

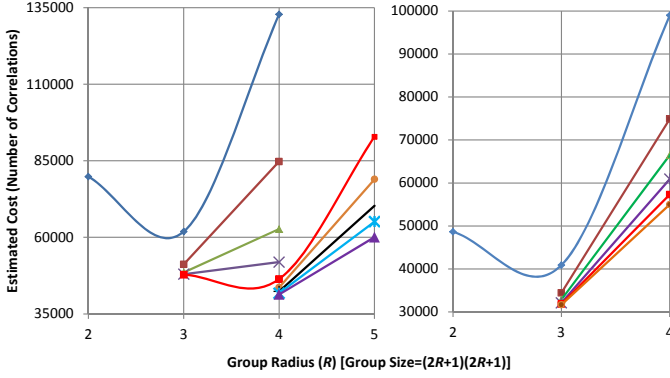


Fig. 4. Each curve is an iteration of OptA algorithm and shows variation of total cost (C_t^k) with group size by using EGS algorithm. In the consecutive iterations of OptA algorithm, minimum cost given by EGS algorithm decreases. Two different scenarios are shown. Fig. 4a: Group size changed from 7×7 to 9×9 Fig. 4b: Group size remained 7×7 . To reduce the number of iterations, algorithm is stopped when $C_t^k - C_t^{k-1} < 0.005C_t^k$.

computation of $\hat{\rho}_{oo}$ given in algorithm 3. Image locations where inequality (28) is not satisfied blurring is not applied and the original image contents are preserved.

C. Loss of Localization

Loss of localization is recovered by introducing a second matching stage in which t is matched with I only in a small neighborhood around the position of ρ_{max} in \hat{I} . We use the size of this neighborhood the same as the size of the blur support $(2d + 1) \times (2d + 1)$.

V. OPTIMIZING AUTO-CORRELATION (OPTA) ALGORITHM

Auto-correlation between two blurred image blocks increases due to variance reduction and also because of the increased overlap in the blur support. Increased auto-correlation makes the transitive bounds tight, resulting in more search locations to be discarded. Algorithm 3 shows how we use non-uniform image blur for optimizing auto-correlation to speedup template matching without accuracy degradation.

In the k^{th} iteration the search image from the last iteration \hat{I}_{k-1} is again convoluted with the blur mask w (19). Auto-correlation between the current blurred image \hat{I}_k and the original image I is computed in the matrix \hat{R}_{oo} . All search locations violating the bound given by (24) are unblurred by copying back full block contents from the original image I to the current blurred image \hat{I}_k . Efficient group size and the cost are estimated by using Algorithm 2. If the current cost c_t^k is less than the previous cost c_t^{k-1} by a relatively big margin $> .005C_t^k$, the algorithm continues to the next iteration, otherwise we get the optimal blurred image \hat{I}_e , local auto-correlation matrix R_{co}^e , and the efficient group size values (h_e, w_e) . Fig. 4 shows two plots of cost c_t^k variations within EGS algorithm in consecutive iterations of OptA. Fig. 4a shows 9 iterations of OptA algorithm. In the $k = 6$ iteration, group size increased from 7×7 to 9×9 . In the later iterations, group size remains fixed, however cost reduced due to tightening of transitive bounds. Fig. 4b shows 6 iterations

Algorithm 3 OptA: Optimizing Auto-correlation using EGS algorithm

Input: $I \in \mathcal{R}^{p \times q}$, (m, n) , ρ_{th} , ρ_{max} , (h_o, w_o) , W {filter}

Output: \hat{I}_e , (h_e, w_e) , R_{co}^e , c_t^e

$[h_1, w_1, R_{co}^1, c_t^1] \leftarrow \text{EGS}(I, h_o, w_o, m, n, \rho_{th})$

$c_t^0 \leftarrow mn pq$

$\lambda = \rho_{th} \rho_{max} + \sqrt{1 + \rho_{th}^2 \rho_{max}^2 - (\rho_{th}^2 + \rho_{max}^2)}$

$S_k = \text{Run-Sum}(I, m, n)$

$Q = \text{Run-Sum}(I * I, m, n)$

$\Omega = \sqrt{Q - \frac{1}{mn} S * S}$

$k = 1, \hat{I}_0 = I$ { k is iteration counter}

while ($c_t^k < c_t^{k-1}$) **do**

$\hat{I}_k = \hat{I}_{k-1} \otimes W$ {convolution}

$P = \hat{I}_k * I$ {*, \div are point-wise operators}

$S_{oo} = \text{Run-Sum}(P, m, n)$

$\hat{S}_k = \text{Run-Sum}(\hat{I}_k, m, n)$

$\hat{Q}_k = \text{Run-Sum}(\hat{I}_k * \hat{I}_k, m, n)$

$\hat{\Omega}_k = \sqrt{\hat{Q}_k - \frac{1}{mn} \hat{S}_k * \hat{S}_k}$

$\hat{R}_{oo} = (S_{oo} - \frac{1}{mn} \hat{S}_k * S) \div (\hat{\Omega}_k * \Omega)$

for all (x, y) **do**

if $\hat{R}_{oo}(x, y) < \lambda$ **then**

$\hat{I}_k(x : x + m, y : y + n) \leftarrow I(x : x + m, y : y + n)$

end if

end for

$[h_{k+1}, w_{k+1}, R_{co}^{k+1}, c_t^{k+1}] \leftarrow \text{EGS}(\hat{I}_k, h_k, w_k, m, n, \rho_{th})$

$k \leftarrow k + 1$

end while

$(\hat{I}_e, h_e, w_e, R_{co}^e, c_t^e) \leftarrow (\hat{I}_{k-1}, h_{k-1}, w_{k-1}, R_{co}^{k-1}, c_t^{k-1})$

of OptA algorithm. In each iteration, EGS cost reduced and in the final iteration, cost reduction was insignificant.

The blur correlation (R_{oo}) computation has a complexity of the order of $O(pq)$. The complexity of convolution is $O((2d + 1)^2 pq)$, where d is the blur support. The dominant computational cost in each iteration is for the efficient group size algorithm which is $O(\omega pq)$ as discussed in Section III-D. Therefore, the overall complexity of Algorithm 3 is $O(\kappa \omega pq)$, where κ is the number of iterations of Algorithm 3.

VI. EARLY DETECTION OF THE HIGH THRESHOLD

A high initial threshold at the start of the search process may significantly increase the probability of success of the sufficient elimination condition and significantly reduce the execution time. However, a very high threshold may result in skipping the best match location while a very small value may result in increased computational cost. In the previous version of TEA [28] the initial threshold was a user defined parameter. We propose a simple strategy to automatically find a suitable threshold value. In the previous TEA, the search space was scanned only once. For each group, the template was matched with the group center and the bounds were computed for the remaining patches in the group. All patches for which the elimination test failed were processed before moving to the next group. As a result, the search space was required to be scanned only once. In contrast, we propose two scans of

TABLE I
SIZE OF TEMPLATE IMAGES $m \times m$ PIXELS AND THE NUMBER OF IMAGES N FOR DIFFERENT DATASETS SHOWN IN FIGURES 5 AND 6

| | | Satellite Image (SI) dataset | | | | | | | | | |
|-----|-----|------------------------------|-----|-----|-----|-----|-----|-----|-----|-----|-----|
| m | 21 | 31 | 41 | 51 | 61 | 71 | 81 | 91 | 101 | 111 | 121 |
| N | 193 | 197 | 198 | 197 | 198 | 197 | 197 | 197 | 200 | 196 | 198 |
| | | Aerial Image (AI) Dataset | | | | | | | | | |
| m | 29 | 39 | 49 | 59 | 69 | 79 | 89 | 99 | 109 | 119 | 129 |
| N | 153 | 175 | 184 | 190 | 198 | 195 | 196 | 199 | 198 | 198 | 200 |

the search space. During the first scan, the template is only matched with the group centers and the maximum correlation value is tracked. Once all group centers are exhausted, the maximum value of the central correlation is used as initial threshold in the second scan.

VII. EXPERIMENTS AND RESULTS

In order to test the proposed fast template matching algorithms, we have performed extensive experimentation on real satellite and aerial image datasets. Performance of the proposed Efficient Group Size (EGS) algorithm and the Optimal Auto-correlation (OptA) algorithm (with efficient group size) is separately reported. Both of these algorithms include the proposed strategy for early detection of the high initial threshold. EGS and OptA are compared with six current algorithms including previous TEA [28], PCE [27], FFT [32], ZEBEC [33], AMWU [34], SAD based on Successive Elimination and Partial Distortion Elimination [35]. The execution time comparisons are performed on Intel Core i3 CPU 2.10GHz and 3.00GB RAM.

Experiments are performed on satellite image dataset (SI) of a low population density seaport (Fig. 5) and aerial image dataset (AI) of a densely populated area (Fig. 6). For each of the two datasets, templates of 11 different sizes are used (Table 1). Total number of templates in the SI dataset are 2168 and in the AI dataset are 2086. The templates are obtained from a different view point at a different time. Therefore both datasets contain projective distortions as well as illumination variations. The dataset, C++ code and the experimental setup will soon be made publicly available at www.csse.uwa.edu.au/~arifm/OptA.htm.

The OptA (Algorithm 3) is executed by varying $W = \{0.05, 0.20, 0.50, 0.20, 0.05\}$, $\rho_{th} = 0.80$ and $\rho_{max} = \{1.0, .95, .90\}$. The algorithm is not much sensitive to ρ_{max} because the image regions with more initial blur start failing the Proposition 4.3 and blurring is stopped in those regions. Therefore, the three values of ρ_{max} resulted in approximately the same optimized auto-correlation. The results in Tables II and III are reported for $\rho_{max} = 0.95$.

In the comparison of OptA with EGS, we observe that OptA has outperformed EGS in all experiments with a maximum speedup of 2.46 times. No loss of accuracy is observed in the OptA algorithm. Maximum localization error is observed up to $\pm(4, 4)$ pixels. Both EGS and OptA algorithms outperformed existing TEA [28] (group size 5×5 and $\rho_{th} = 0.80$) on all datasets (Tables II and III). OptA has obtained maximum 3 times speedup over TEA and on the average, 2.7% more elimination on AI dataset (Table IV).



Fig. 5. Satellite Image (SI) dataset: search image is 962×622 pixels and the template images have sizes varying from 21×21 to 121×121 .



Fig. 6. Aerial Image (AI) dataset: search image is 1549×2389 pixels and the template images vary from 29×29 to 129×129 pixels.

TABLE II
TOTAL EXECUTION TIME (SEC) INCLUDING ALL RELATED OVERHEADS ON SATELLITE IMAGE (SI) DATASET. THE PROPOSED ALGORITHMS OPTA AND EGS ARE COMPARED WITH FIVE EXISTING TECHNIQUES

| m | OptA | EGS | TEA | PCE | ZEBEC | FFT | SAD |
|-----|------|-----|-----|-----|-------|-----|-----|
| 21 | 10 | 11 | 13 | 17 | 32 | 128 | 26 |
| 31 | 13 | 15 | 20 | 25 | 114 | 134 | 59 |
| 41 | 17 | 18 | 26 | 42 | 148 | 137 | 96 |
| 51 | 23 | 25 | 38 | 53 | 80 | 133 | 156 |
| 61 | 28 | 31 | 47 | 66 | 253 | 131 | 216 |
| 71 | 38 | 40 | 58 | 80 | 308 | 301 | 303 |
| 81 | 46 | 48 | 65 | 93 | 101 | 311 | 406 |
| 91 | 54 | 57 | 78 | 110 | 123 | 317 | 492 |
| 101 | 67 | 70 | 89 | 127 | 427 | 327 | 596 |
| 111 | 72 | 76 | 97 | 144 | 206 | 337 | 681 |
| 121 | 84 | 87 | 110 | 161 | 175 | 313 | 810 |

TABLE III
TOTAL EXECUTION TIME (SEC) ON AERIAL IMAGE (AI) DATASET. THE PROPOSED ALGORITHMS OPTA AND EGS ARE COMPARED WITH FIVE EXISTING TECHNIQUES.

| m | OptA | EGS | TEA | PCE | ZEBC | FFT | SAD |
|-----|------|-----|-----|------|------|------|------|
| 29 | 55 | 69 | 76 | 121 | 456 | 1138 | 226 |
| 39 | 82 | 97 | 117 | 234 | 277 | 1288 | 472 |
| 49 | 123 | 139 | 175 | 336 | 277 | 1337 | 798 |
| 59 | 126 | 189 | 237 | 450 | 1203 | 1372 | 1212 |
| 69 | 146 | 238 | 300 | 554 | 250 | 1481 | 1839 |
| 79 | 172 | 300 | 356 | 651 | 1639 | 1442 | 2371 |
| 89 | 205 | 367 | 426 | 795 | 1869 | 1423 | 3108 |
| 99 | 245 | 451 | 500 | 983 | 833 | 1423 | 3960 |
| 109 | 214 | 526 | 580 | 1120 | 2356 | 1436 | 4794 |
| 119 | 225 | 380 | 661 | 1278 | 2575 | 1413 | 5727 |
| 129 | 253 | 422 | 757 | 1470 | 3074 | 1456 | 6822 |

TABLE IV
AVERAGE PERCENT COMPUTATION ELIMINATION ON THE SI AND AI DATASETS

| Dataset | OptA | EGS | TEA | PCE | ZEBC | SAD |
|---------|------|------|------|------|------|------|
| SI | 94.5 | 94 | 91.9 | 87.5 | 95.7 | 66.4 |
| AI | 96.7 | 95.2 | 94 | 87.2 | 95.2 | 68.3 |

OptA outperformed PCE [27] (initial partitions= m , $\rho_{th} = 0.80$, two-stage initialization strategy) on all datasets obtaining maximum speedup of 7.13 times and average computation elimination up to 9.5% on AI dataset. This experiment demonstrates significant improvement over current state of the art algorithm.

The OptA outperformed ZEBC [33] with relatively bigger margins. For ZEBC, the partition parameter (r) is kept close to 8 and $\rho_{th} = 0.80$ as recommended by [33]. Since the template rows must be divisible by r , for each experiment the most efficient value of r is chosen. Maximum speedup of OptA over ZEBC is 12.13 times. On SI dataset ZEBC obtained higher computation elimination. However due to the larger cost of the elimination test, ZEBC was not able to get the benefit of high computation elimination. We have also compared OptA with FFT [32] and we observe up to 22.04 times speed up. Speed up over FFT is generally larger for smaller template sizes and lesser for the larger sizes. It is because the computational cost of FFT has relatively less variation with template size increments.

For the three AI dataset 29×29 , 39×39 , and 49×49 initial threshold is varied as $\{0.70, 0.75, 0.80, 0.85, 0.90\}$ and the variation of total execution time over these two datasets for the OptA algorithm is observed as $\{294, 287, 287, 287, 286\}$ seconds respectively. The execution time is almost constant for the threshold ≥ 0.75 . This experiment shows that the sensitivity of the proposed algorithm to the initial threshold is low.

The proposed algorithm (OptA) is also compared with AMWU [34]. For this comparison, we prepared two new AI datasets with template sizes 32×32 and 64×64 , because AMWU requires the template dimensions to be in the powers of 2. For the AI reference of size 1549×2389 , AMWU is

more than an order of magnitude slower than our proposed algorithm. AMWU is much efficient on the small search space $\leq 512 \times 512$ [34], however for the large search space, its performance degrades probably significantly long lists of the temporary winners make the hashing scheme inefficient.

Among the two datasets, OptA obtained more speed up on the AI dataset mainly because it contains significant details and high frequency contents. OptA was able to induce blurring at most of the AI reference image locations without loss of image quality. Less speedup on SI dataset is because a big portion of SI reference image is sea, having no details. OptA was not able to blur that portion because blurring caused image quality degradation.

In both datasets ground truth was manually marked and a match was considered correct if it was within $(\pm 4, \pm 4)$ pixels of the ground truth location. Using this criterion, OptA and EGS exhibited 100% accuracy on all datasets while SAD has an average accuracy of 81.0% over AI and 76.11% over SI datasets. Maximum speedup of OptA over SAD with SEA and PDE is 26.93 times. Although more efficient implementations of SAD exist, however accuracy of SAD cannot be improved over the exhaustive accuracy.

VIII. CONCLUSION

A fast template matching system was proposed to find a target in a large search space. Fast match speedup was obtained by inducing non uniform blur in the search space. Exhaustive math accuracy was ensured by maintaining a minimum image quality at all locations. For this purpose an Optimal Auto-correlation (OptA) algorithm was proposed. OptA algorithm was based on Efficient Group Size (EGS) algorithm which made the transitive elimination algorithm more efficient. Moreover, a technique for early detection of the high initial threshold was also proposed. The fast template matching system was compared with six existing algorithms on two different datasets. The proposed system consistently outperformed the existing techniques.

IX. ACKNOWLEDGEMENTS

This research was supported by Australian Research Council grants DP1096801 and DP110102399.

REFERENCES

- [1] S. Rousseau, D. Helbert, P. Carre, and J. Blanc-Talon, "Compressive pattern matching on multispectral data," *Geoscience and Remote Sensing, IEEE Transactions on*, vol. 52, no. 12, pp. 7581–7592, Dec 2014.
- [2] Y. Bentoutou, N. Taleb, K. Kpalma, and J. Ronsin, "An automatic image registration for applications in remote sensing," *Geoscience and Remote Sensing, IEEE Transactions on*, vol. 43, no. 9, pp. 2127–2137, Sept 2005.
- [3] R. Caves, P. Harley, and S. Quegan, "Matching map features to synthetic aperture radar (sar) images using template matching," *Geoscience and Remote Sensing, IEEE Transactions on*, vol. 30, no. 4, pp. 680–685, Jul 1992.
- [4] X. Chen, J. Guan, Z. Bao, and Y. He, "Detection and extraction of target with micromotion in spiky sea clutter via short-time fractional fourier transform," *Geoscience and Remote Sensing, IEEE Transactions on*, vol. 52, no. 2, pp. 1002–1018, Feb 2014.
- [5] J. Ma, J. Chan, and F. Canters, "Fully automatic subpixel image registration of multiangle chris/proba data," *Geoscience and Remote Sensing, IEEE Transactions on*, vol. 48, no. 7, pp. 2829–2839, July 2010.

- [6] L. Bandeira, J. Saraiva, and P. Pina, "Impact crater recognition on mars based on a probability volume created by template matching," *Geoscience and Remote Sensing, IEEE Transactions on*, vol. 45, no. 12, pp. 4008–4015, Dec 2007.
- [7] R. Mayer, F. Bucholtz, and D. Scribner, "Object detection by using "whitening/dewhitening" to transform target signatures in multitemporal hyperspectral and multispectral imagery," *Geoscience and Remote Sensing, IEEE Transactions on*, vol. 41, no. 5, pp. 1136–1142, May 2003.
- [8] M. Dufour, L. Miller, and P. Galatsanos, "Template matching based object recognition with unknown geometric parameters," *Image Processing, IEEE Transactions on*, vol. 11, no. 12, pp. 1385–1396, 2002.
- [9] M. Uss, B. Voze, V. Dushepa, V. Komjak, and K. Chehdi, "A precise lower bound on image subpixel registration accuracy," *Geoscience and Remote Sensing, IEEE Transactions on*, vol. 52, no. 6, pp. 3333–3345, June 2014.
- [10] L. Brown, "A survey of image registration techniques," *ACM Computing Surveys*, vol. 24, pp. 326–373, 1992.
- [11] Y. Ahn and I. Howat, "Efficient automated glacier surface velocity measurement from repeat images using multi-image/multichip and null exclusion feature tracking," *Geoscience and Remote Sensing, IEEE Transactions on*, vol. 49, no. 8, pp. 2838–2846, Aug 2011.
- [12] A. Evans, "Glacier surface motion computation from digital image sequences," *Geoscience and Remote Sensing, IEEE Transactions on*, vol. 38, no. 2, pp. 1064–1072, Mar 2000.
- [13] X. Hu, Y. Li, J. Shan, J. Zhang, and Y. Zhang, "Road centerline extraction in complex urban scenes from lidar data based on multiple features," *Geoscience and Remote Sensing, IEEE Transactions on*, vol. 52, no. 11, pp. 7448–7456, Nov 2014.
- [14] S. Gibbons and F. Ringdal, "Seismic monitoring of the north korea nuclear test site using a multichannel correlation detector," *Geoscience and Remote Sensing, IEEE Transactions on*, vol. 50, no. 5, pp. 1897–1909, May 2012.
- [15] H. Zhang, K. Sun, and W. Li, "Object-oriented shadow detection and removal from urban high-resolution remote sensing images," *Geoscience and Remote Sensing, IEEE Transactions on*, vol. 52, no. 11, pp. 6972–6982, Nov 2014.
- [16] G. Vivone, P. Addesso, R. Conte, M. Longo, and R. Restaino, "A class of cloud detection algorithms based on a map-mrf approach in space and time," *Geoscience and Remote Sensing, IEEE Transactions on*, vol. 52, no. 8, pp. 5100–5115, Aug 2014.
- [17] A. Komarov and D. Barber, "Sea ice motion tracking from sequential dual-polarization radarsat-2 images," *Geoscience and Remote Sensing, IEEE Transactions on*, vol. 52, no. 1, pp. 121–136, Jan 2014.
- [18] A. Berg and L. Eriksson, "Investigation of a hybrid algorithm for sea ice drift measurements using synthetic aperture radar images," *Geoscience and Remote Sensing, IEEE Transactions on*, vol. 52, no. 8, pp. 5023–5033, Aug 2014.
- [19] V. N. Radhika, B. Kartikeyan, B. Gopala Krishna, S. Chowdhury, and P. Srivastava, "Robust stereo image matching for spaceborne imagery," *Geoscience and Remote Sensing, IEEE Transactions on*, vol. 45, no. 9, pp. 2993–3000, Sept 2007.
- [20] H. Fujisada, M. Urai, and A. Iwasaki, "Advanced methodology for aster dem generation," *Geoscience and Remote Sensing, IEEE Transactions on*, vol. 49, no. 12, pp. 5080–5091, Dec 2011.
- [21] J. Piedra-Fernandez, G. Ortega, J. Wang, and M. Canton-Garbin, "Fuzzy content-based image retrieval for oceanic remote sensing," *Geoscience and Remote Sensing, IEEE Transactions on*, vol. 52, no. 9, pp. 5422–5431, Sept 2014.
- [22] D. Espinoza-Molina and M. Datcu, "Earth-observation image retrieval based on content, semantics, and metadata," *Geoscience and Remote Sensing, IEEE Transactions on*, vol. 51, no. 11, pp. 5145–5159, Nov 2013.
- [23] Y. Hel-Or and H. Hel-Or, "Real-time pattern matching using projection kernels," *IEEE Trans. Pattern Anal. Machine Intell.*, vol. 27, no. 9, pp. 1430–1445, September 2005.
- [24] W. Ouyang, F. Tombari, S. Mattoccia, L. Di Stefano, and W.-K. Cham, "Performance evaluation of full search equivalent pattern matching algorithms," *Pattern Analysis and Machine Intelligence, IEEE Transactions on*, vol. 34, no. 1, pp. 127–143, 2012.
- [25] F. Tombari, S. Mattoccia, and L. Di Stefano, "Full-search-equivalent pattern matching with incremental dissimilarity approximations," *Pattern Analysis and Machine Intelligence, IEEE Transactions on*, vol. 31, no. 1, pp. 129–141, 2009.
- [26] S. Mattoccia, F. Tombari, and L. Di Stefano, "Fast full-search equivalent template matching by enhanced bounded correlation," *IEEE Trans. Image Processing*, vol. 17, no. 4, pp. 528–538, 2008.
- [27] A. Mahmood and S. Khan, "Correlation-coefficient-based fast template matching through partial elimination," *IEEE Trans. Image Proc.*, vol. 21, no. 4, pp. 2099–2108, april 2012.
- [28] —, "Exploiting transitivity of correlation for fast template matching," *IEEE Transactions on Image Processing*, vol. 19, no. 8, pp. 2190–2200, August 2010 2010.
- [29] J. S. Cramer, "Mean and variance of r^2 in small and moderate samples," *Journal of Econometrics*, vol. 35, no. 2, pp. 253–266, 1987.
- [30] M. L. Carrodus and D. E. Giles, "The exact distribution of r^2 when the regression disturbances are autocorrelated," *Economics Letters*, vol. 38, no. 4, pp. 375–380, 1992.
- [31] J. Koerts and A. P. J. Abrahamse, *On the theory and application of the general linear model*. Rotterdam University Press Rotterdam, 1969.
- [32] P. William, T. Saul, V. William, and F. Brian, *Numerical Recipes: The Art of Scientific Computing*, 3rd ed. Cambridge University Press, 2007.
- [33] S. Mattoccia, F. Tombari, and L. Di Stefano, "Reliable rejection of mismatching candidates for efficient ZNCC template matching," in *ICIP*. IEEE, 2008, pp. 849–852.
- [34] S.-D. Wei and S.-H. Lai, "Fast template matching based on normalized cross correlation with adaptive multilevel winner update," *Image Processing, IEEE Transactions on*, vol. 17, no. 11, pp. 2227–2235, 2008.
- [35] B. Montrucchio and D. Quaglia, "New sorting-based lossless motion estimation algorithms and a partial distortion elimination performance analysis," *IEEE Trans. Circuits Syst. Video Technol.*, vol. 15, no. 2, pp. 210–220, 2005.